Supporting Information for "A robust method for selecting a high-quality interferogram subset in InSAR surface deformation analysis"

M. S. Zebker [1] *, J. Chen[1,2]

[1]Jackson School of Geoscience, Department of Earth and Planetary Science, The University of Texas at Austin, Austin, TX

[2]Department of Aerospace Engineering and Engineering Mechanics, The University of Texas at Austin, Austin, TX

Contents of this file

1. Section S1
2. Tables S1 to S3
3. Figures S1 to S3

Corresponding author: M. S. Zebker, Department of Earth and Planetary Science, The University of Texas at Austin, Austin, TX, 78712, USA. mzebker@utexas.edu

*Austin, TX

S1. Residual tropospheric noise in Small BAseline Subset solutions

Under the assumption that tropospheric turbulence noise is the primary error source, the observed InSAR phase, $\Delta\phi$, at a pixel of interest can be defined as:

$$\Delta\phi = \frac{4\pi}{\lambda}(\Delta d + \Delta n) \tag{1}$$

where λ is the radar wavelength, Δd is the line-of-sight (LOS) deformation between the two radar acquisition times, and Δn is the tropospheric turbulence noise at this pixel location.

Given M SAR acquisitions, we can form N high-quality interferograms. To compute the average velocity, v_c, over the study period, we define an SBAS system of N equations as:

$$BPv_c = \Delta\Phi \tag{2}$$

where B is the $N \times (M-1)$ system matrix as defined in Berardino, Fornaro, Lanari, and Sansosti (2002). P is a $(M-1) \times 1$ vector of ones, and $\Delta\Phi = [\Delta\phi_1, ..., \Delta\phi_N]^T$ is a $N \times 1$ vector of observed phases at the pixel of interest. The least squares solution for v_c is:

$$\begin{aligned} v_c &= \frac{\lambda}{4\pi \sum_i^N \Delta t_i^2} \sum_i^N \Delta t_i \Delta\phi_i \\ &= \frac{\lambda}{4\pi \sum_i^N \Delta t_i^2} \sum_i^N \Delta t_i \Delta d_i + \frac{\lambda}{4\pi \sum_i^N \Delta t_i^2} \sum_i^N \Delta t_i \Delta n_i \end{aligned} \tag{3}$$

where Δt_i is the temporal baseline of the interferogram i. The residual tropospheric noise, r_n, in the SBAS constant velocity solution is:

$$r_n = \frac{\lambda}{4\pi \sum_i^N \Delta t_i^2} \sum_i^N \Delta t_i \Delta n_i \tag{4}$$

A smaller noise residual leads to a more accurate velocity solution. Based on Eq. 4, the residual tropospheric noise is smaller when interferograms with longer temporal baselines are used as input in the SBAS inversion. For example, for the same N, the residual tropospheric noise is four times smaller if all interferograms span 48 days instead of 12 days. Furthermore, the residual noise tends to decrease when N increases, given that tropospheric turbulence noise can be considered random over time.

References

Berardino, P., Fornaro, G., Lanari, R., & Sansosti, E. (2002). A new algorithm for surface deformation monitoring based on small baseline differential SAR interferograms. *IEEE Transactions on Geoscience and Remote Sensing*, *40*(11), 2375-2383. doi: 10.1109/TGRS.2002.803792

Table S1. Time (in seconds) required for unwrapping original and reconstructed interferograms (Fig. 2) over the Eagle Ford site.

Interferogram	Original	Reconstructed
20180805-20180910	1	1
20180817-20181016	227	9
20190520-20190812	178	5
20180525-20180910	83	1
20200526-20210602	147	2
20180618-20190929	181	3
20191023-20191222	<1	1
20191128-20200327	2	1
20170331-20171208	209	19
20201029-20211223	165	3
20191011-20201228	156	2
20200127-20210427	192	5

Table S2. InSAR-GPS line-of-sight misfit (mm/yr) for different deformation solutions at 24 California GPS stations.

GPS Station	New Workflow	SBAS-12	SBAS-48	SBAS-180	SBAS-360	SBAS-1000
CACO	3.7	15.9	4.4	2.3	2.1	3.8
CAD1	-3.0	-17.8	-5.7	-1.0	1.4	3.3
CAFP	-0.8	-5.8	-1.8	6.8	8.0	-16.4
CAHA	-9.1	-18.6	-9.7	-14.0	-20.6	-49.6
CAKC	2.9	9.6	4.4	1.6	2.7	3.3
CAWO	-4.5	1.2	-5.9	-5.6	-2.1	0.3
CRCN	-1.9	-21.2	-0.2	0.6	-10.5	-55.2
DLNO	-2.5	-14.2	-4.3	-1.2	0.2	1.7
GR8R	-1.0	8.9	-1.3	0.6	0.6	2.4
LEMA	-6.7	-15.6	-6.2	-9.2	-14.1	-41.9
MULN	-2.1	-0.6	-1.0	-3.3	4.0	-5.5
P056	-6.4	-12.3	-2.6	-9.7	-17.3	-30.5
P300	1.6	3.6	-0.2	2.5	2.9	4.5
P302	4.1	23.5	1.0	3.6	3.5	6.0
P304	4.0	29.2	2.1	-4.7	3.9	5.9
P541	2.9	13.5	2.5	3.6	3.5	4.9
P547	1.1	25.5	-1.3	0.7	0.3	1.3
P564	2.3	-15.3	-2.0	-8.0	-5.3	-5.8
P565	-1.7	-18.8	-4.9	-1.6	0.4	2.5
P566	-3.9	-4.5	-7.0	-5.8	-3.7	-9.4
P809	-2.6	-19.6	-5.8	-2.5	-0.5	1.7
P810	-1.9	-19.0	-5.2	-1.8	0.2	2.3
RAPT	-4.7	3.8	-6.7	-5.2	-1.3	5.2
TRAN	7.1	15.8	2.8	7.8	16.9	12.4
MAE	3.4	13.9	3.7	4.3	5.2	11.5

Table S3. InSAR-GPS line-of-sight misfit (mm/yr) for different deformation solutions at 5 Texas GPS stations.

GPS Station	New Workflow	SBAS-12	SBAS-24	SBAS-48	SBAS-96	SBAS-180
LCNX	-2.4	-1.3	1.5	-8.6	-14.1	-13.9
TXCU	4.8	-16.0	12.5	28.1	35.3	34.7
TXKC	3.5	0.1	4.9	12.6	13.2	16.8
TXFV	0.7	2.8	-0.3	0.0	-1.1	-0.7
TXFI	2.1	-7.4	-4.3	-2.8	-1.0	0.5
MAE	2.7	5.5	4.7	10.4	12.9	13.3

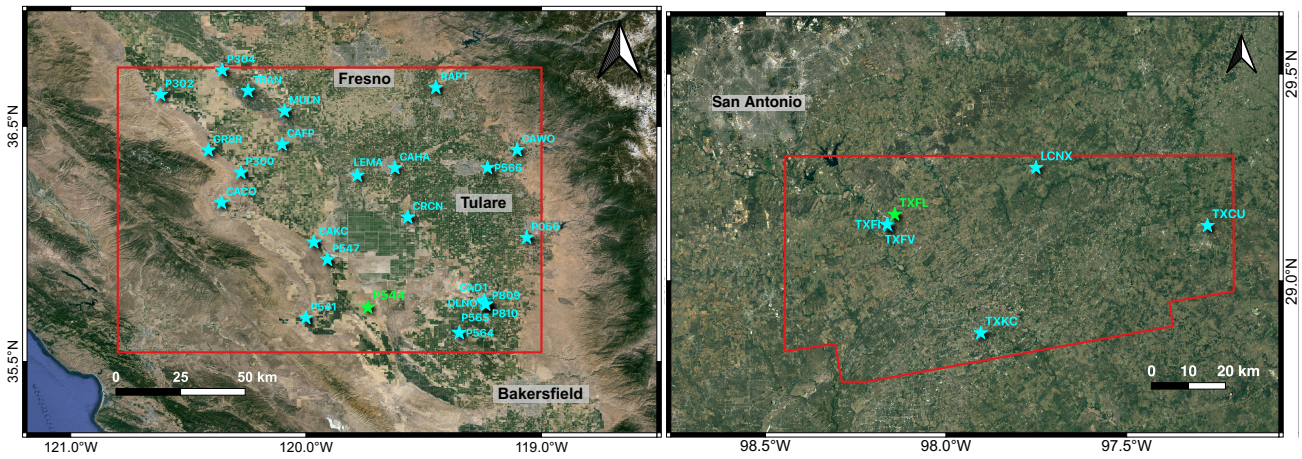

Figure S1. (Left) Tulare Basin and (Right) Eagle Ford study sites. The radar footprints are outlined in red, the reference GPS stations are shown as green stars, and GPS validation stations are shown as blue stars.

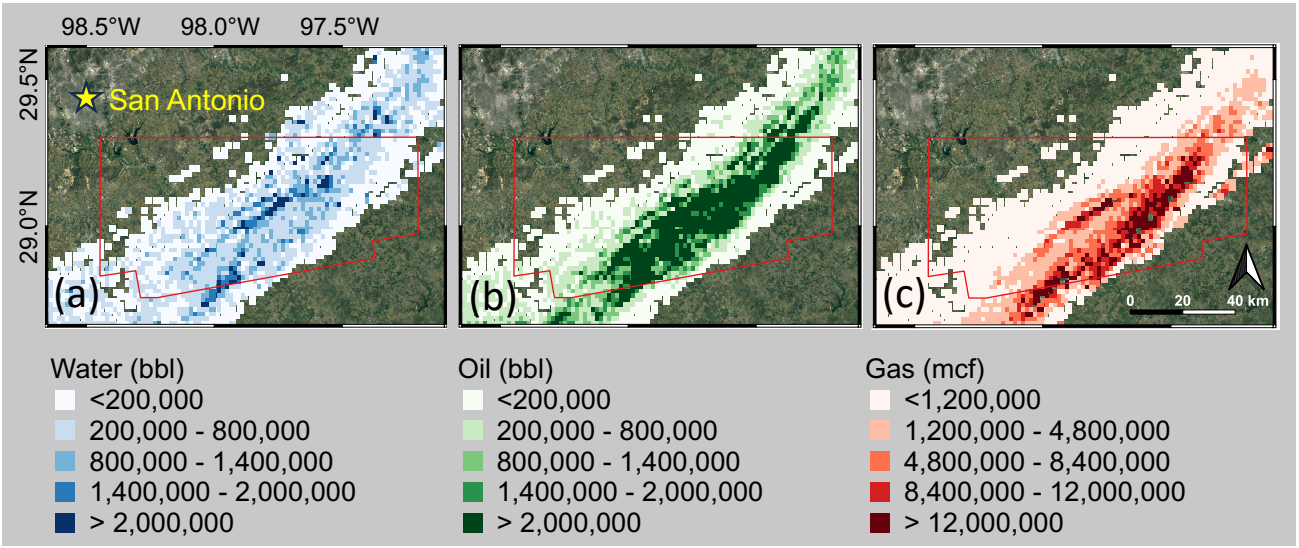

Figure S2. Cumulative water, oil, and gas production over the Eagle Ford region from 1974-2022, where over 90% of total production has occurred since 2010. The outline of the radar footprint is in red. Produced water, oil, and gas data provided by Center for Injection and Seismicity Research (CISR) at The University of Texas at Austin, Bureau of Economic Geology (BEG).

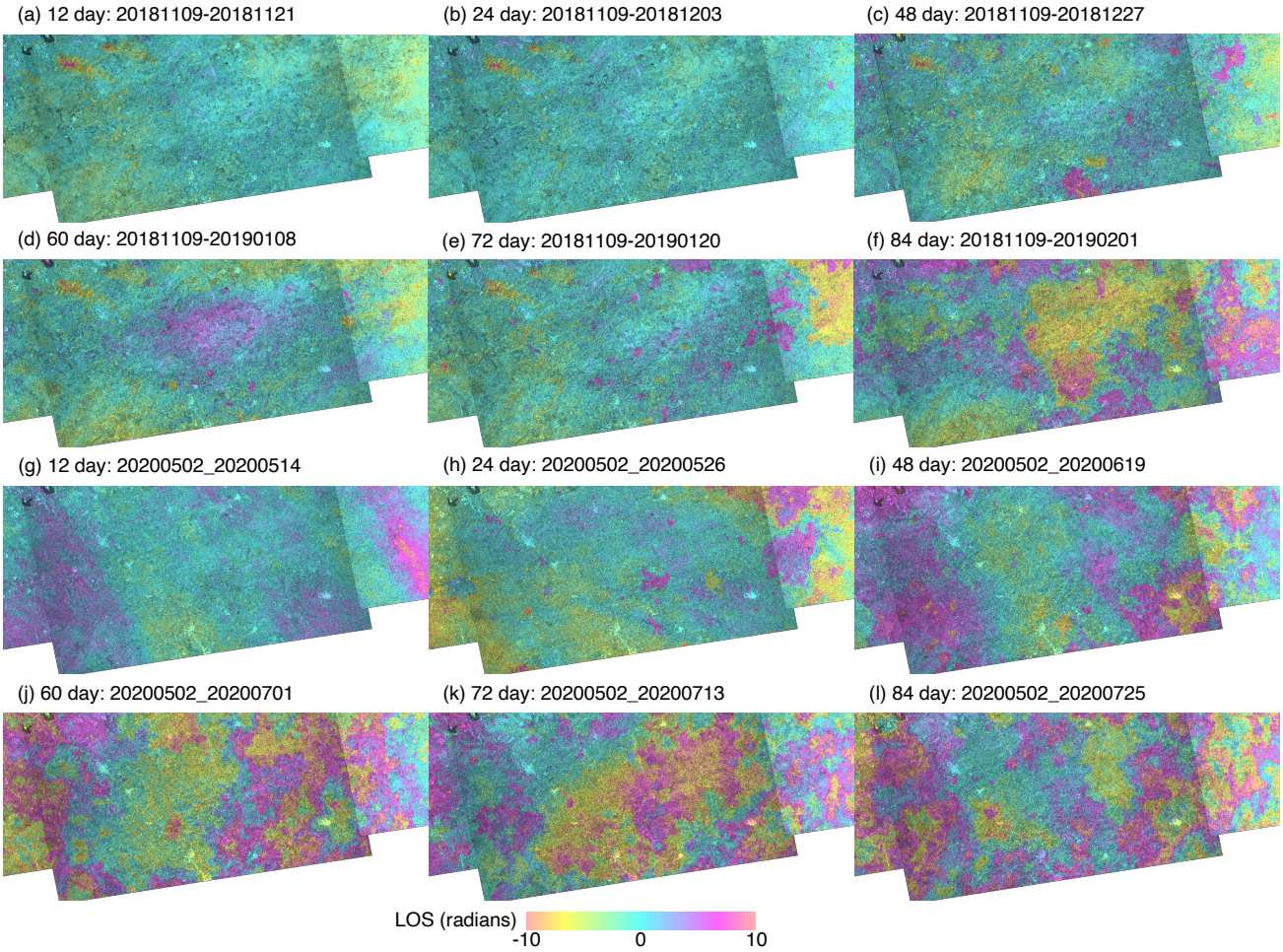

Figure S3. Eagle Ford interferograms that span the winter months (a-f) and summer months (g-l) with varying temporal baselines. Over the winter months, unwrapping errors occur in interferograms that span 48 days or longer, while over the summer months, unwrapping errors occur in interferograms that span 24 days or longer.